Photonic realization of a transition to a strongly driven Floquet topological phase

Jonathan Guglielmon, Sheng Huang, Kevin P. Chen, and Mikael C. Rechtsman

Phys. Rev. A **97**, 031801 — Published 30 March 2018

DOI: 10.1103/PhysRevA.97.031801

Photonic realization of a transition to a strongly driven Floquet topological phase

Jonathan Guglielmon[1], Sheng Huang[2], Kevin P. Chen[2], and Mikael C. Rechtsman[1]
[1] *Department of Physics, The Pennsylvania State University, University Park, Pennsylvania 16802, USA*
[2] *Department of Electrical and Computer Engineering, University of Pittsburgh, Pittsburgh, Pennsylvania 15261, USA*
(Dated: March 12, 2018)

Floquet systems provide a platform with significant potential for generating and controlling topological phases of matter. By introducing an external driving field, a topologically trivial system can be driven to topological phases possessing non-zero bulk invariants and associated gapless surface modes. One rich feature of Floquet systems is that, as one moves away from the weak field regime by increasing the amplitude of the driving field, one can encounter a series of topological transitions which place the system in distinct topological phases. Here we experimentally demonstrate this phenomenon in a photonic system consisting of an array of evanescently-coupled helical waveguides. We show that by moving between the weakly and strongly driven regimes, we can induce a transition in which the bulk topological invariant changes sign and the associated topological edge mode reverses its propagation direction. These two topological phases are part of a larger phase diagram and serve to demonstrate both the rich topological physics present in Floquet systems as well as the accessibility of the strongly driven regime—a regime typically associated with the difficulties of large radiative losses for photonic systems and significant heating for their condensed matter counterparts.

In recent years, the field of condensed matter physics has been profoundly impacted by the discovery of topological insulators, a state of matter in which the global, topological structure of the system's eigenstates results in surprisingly robust properties. Though originally discovered in the condensed matter context, many of the underlying topological ideas have since been realized in a variety of other settings including photonic [1–6], ultracold atomic [7–9], and mechanical systems [10–14]. In addition to potentially enabling unique device functionalities within these fields, the advent of topological physics in these settings provides a platform for the experimental realization of topological phenomena in a context where it is possible to directly engineer the microscopic details of the system, including the underlying lattice, the interactions, and the structure of any applied gauge fields.

A particularly interesting example in photonics is provided by paraxial waveguide arrays [15], where the physics of paraxial light diffracting through a collection of evanescently-coupled waveguides is identical to the physics of a non-interacting electron confined to two dimensions evolving according to the Schrödinger equation. While for electrons the Hamiltonian generates evolution in time, for photons it generates evolution along the paraxial spatial direction (i.e., the propagation axis of the waveguides). This map from temporal to spatial degrees of freedom can be exploited to explore Floquet phenomena associated with intricate time-dependent Hamiltonians. This provides a particularly fruitful avenue for obtaining topological systems in photonics, since it is known that Floquet systems can exhibit topologically non-trivial phases [16–19]. Furthermore, this gives rise to novel effects that can be explored in the context of Floquet topological physics related to the fact that photons are bosons, and that photonic systems are by nature strongly out of equilibrium.

A photonic realization of such a Floquet topological insulator was given in [3] where a honeycomb array of helical waveguides was fabricated such that the waveguide helicity generates an effective gauge field that drives the system to a topologically non-trivial phase. In that experiment, the observed topological phase resides in the weak field regime where the gauge field amplitude is small and the chirality of the helices determines the chirality of the topological edge mode. Moving beyond this regime by ramping up the amplitude of the gauge field can lead to an intricate series of topological phase transitions. More generally, the combination of the amplitude and frequency degrees of freedom provides a two-dimensional parameter space that has been shown, in the condensed matter context, to result in a surprisingly rich phase diagram [20].

In this paper, we move into the strongly driven regime of that phase diagram, where we observe a phase in which the Floquet topological winding number [21] changes sign relative to the weakly driven phase and the associated topological edge mode reverses its propagation direction so that its chirality is opposite to the chirality of the helices (we use the winding number here instead of the Chern number since it is the appropriate bulk invariant for Floquet systems [21]). Our observation provides an experimental demonstration of the potential for using the degrees of freedom associated with the Floquet drive amplitude to tune a system's topological phase.

A complication encountered in the strongly driven regime is the problem of waveguide bending loss (equivalent to the problem of overheating in condensed matter), an effect that inhibited observation of a phase transition in prior experimental studies [3]. We find that this problem can be circumvented by working in the highly irregular parameter regime in which the helix diameter is on the same scale as the size of the entire waveguide array. While a photonic topological transition has been demonstrated previously [22, 23] (from topological to trivial),

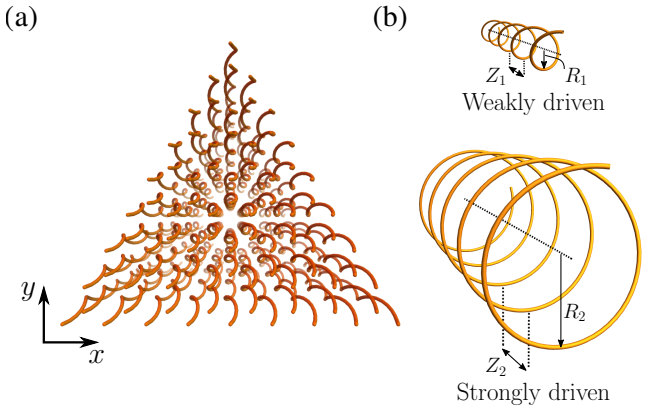

FIG. 1. (a) Illustration of our honeycomb array of helical waveguides. Light is injected at the front of the structure and evolves in the transverse plane as it propagates into the page along the z-direction. (b) Isolated waveguides highlighting the parameters (R, Z), which respectively specify the helix radius and helix period. By varying these parameters, we can place the system in a variety of topological phases. The upper and lower panels respectively illustrate the waveguides used in realizing the weakly and strongly driven topological phases discussed in the text.

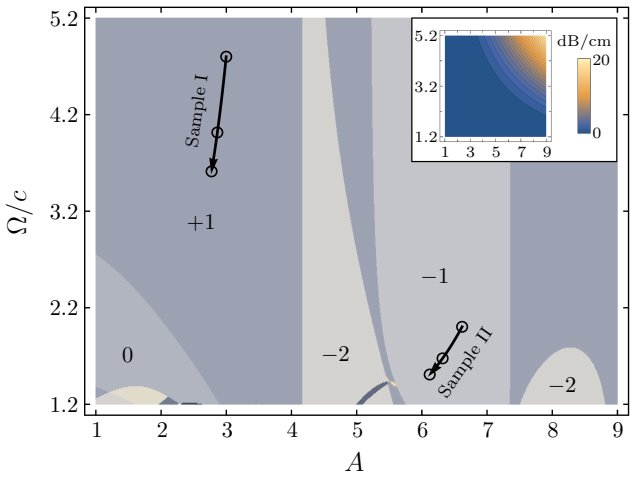

FIG. 2. Floquet topological phase diagram showing the winding number associated with the $\beta = 0$ gap as a function of the dimensionless parameters Ω/c and A. Each region has been colored according to the value of the winding number and corresponding numerical labels have been added to the key regions. Inset shows a theoretical estimate of the bending loss plotted on axes identical to those of the phase diagram. The regions of the phase diagram probed in our experiment are labeled 'Sample I' and 'Sample II' residing, respectively, in the weakly driven and strongly driven regimes. Shown alongside the labels is an arrow that indicates the path taken by a wavelength sweep from 1480 nm to 1600 nm. The three points highlighted along the path correspond to the wavelengths of Fig. 4.

the effect we study here is clearly distinct both in that our transition occurs between non-trivial phases with opposite edge mode chirality and in the sense that our result demonstrates the possibility of experimentally accessing the topological features of photonic Floquet systems beyond the regime associated with a weak gauge field. Additionally, the phases studied here can be mapped in an appropriate limit to the Haldane model (i.e., the quantum anomalous Hall effect [24, 25]), highlighting its similarities to the Haldane model while showing that the Floquet system is in fact much richer. Finally, we mention that our system has a close relation to the mathematically equivalent condensed matter system of graphene irradiated by strong, circularly polarized light [16, 19]. We thus show—by analogy with photonics—that the intensity of the irradiating light can be used to tune between topological phases. Like the electronic system, the photonic system is also constrained by 'heating' (i.e., bending loss), and we provide a prescription for overcoming its limitations.

RESULTS

Fig. 1 illustrates our photonic structure, which consists of a honeycomb array of helical waveguides aligned along the z-direction. The helices are characterized by their radius R and their spatial period Z. We also define the helix frequency $\Omega = 2\pi/Z$. In the paraxial approximation, the electric field $\mathbf{E}(x, y, z) = \psi(x, y, z)\exp(ik_0 z - i\omega t)\hat{\mathbf{E}}_0$ is governed by an equation resembling the Schrödinger equation, in which the paraxial direction, z, takes the place of time and the variation, δn, of the refractive index $n = n_0 + \delta n$ plays the role of a potential. Here $\omega = 2\pi c/\lambda$ is the operating frequency, λ is the wavelength, and $k_0 = 2\pi n_0/\lambda$ is the background wavenumber. The waveguides used in our experiment have been engineered to exhibit a single bound mode each for wavelengths in the vicinity of 1550 nm. We choose our lattice constant so that the resulting paraxial Schrödinger equation can be modeled using tight-binding theory where light hops between the bound modes of adjacent waveguides via evanescent coupling. The effect of the helices is to introduce a z-dependent gauge field [3]

$$\mathbf{A}(z) = k_0 R\Omega\,[\sin(\Omega z), -\cos(\Omega z), 0] \tag{1}$$

that modifies the hopping amplitudes with a Peierls phase yielding a tight-binding Schrödinger equation

$$i\partial_z \psi_n(z) = \sum_{\langle m \rangle} c\, e^{i\mathbf{A}(z)\cdot\mathbf{r}_{mn}} \psi_m(z) \tag{2}$$

where ψ_n is the amplitude of the electric field in the n^{th} waveguide, $\mathbf{r}_{mn}$ is the displacement between sites m, n, c is the hopping constant, and the sum over m is taken over nearest neighbors. We will denote the eigenvalues of the Hamiltonian associated with Eq. 2 by β.

In the absence of the gauge field, the tight binding band structure for this system reduces to that of

graphene and possesses two distinct Dirac cones at the corners of the Brillouin zone. The introduction of $\mathbf{A}(z)$ breaks z-reversal symmetry and is thus capable of driving the system to topologically non-trivial phases. Since this is a Floquet system, the appropriate topological invariant is the winding number introduced in [21], which we compute for the gap centered on $\beta = 0$. Here the winding number is fully determined by the two dimensionless parameters Ω/c and $A = ak_0R\Omega$, which correspond to the frequency and amplitude of the gauge field. The resulting phase diagram is shown in Fig. 2, which was computed using the truncated Floquet scheme given in [21] combined with the algorithm of [26]. Note that due to the close relation between our photonic system and the Schrödinger equation, this is the same Floquet topological phase diagram that has been studied in the context of graphene irradiated by circularly-polarized light [20].

For this system, the driving amplitude is a function of both the helix radius and helix frequency: $A = ak_0R\Omega$. Thus, for a fixed helix frequency, an increase in the amplitude A will result in a decrease in the curvature radius $R_c = 1/(R\Omega^2)$ of the waveguides (note the distinction between the curvature radius R_c and the helix radius R). In general, waveguide bending loss increases as R_c is decreased [27] and it was precisely these losses that prohibited the observation of a phase transition in [3]. A key result of this current work is that, by increasing the gauge field amplitude while simultaneously reducing its frequency, the losses can be reduced to a degree that allows us to observe a topological phase residing in the strongly driven regime.

To determine which regions of the phase diagram are excluded from experimental observation due to bending loss, we show in the inset of Fig. 2 the bending loss computed over the same parameter space used in plotting the phase diagram. We note that in mapping the loss over this parameter space, we have assumed a lattice constant of $a = 22\sqrt{3}\,\mu$m. These losses represent a theoretical estimate computed using the result of [27] for light of wavelength 1550 nm by approximating our waveguides as having a circular cross section with a diameter equal to the average of the diameters along the x and y directions. By working in the lower region of the phase diagram, we can reduce the losses to a degree that enables observation of additional topological phases.

To the best of our knowledge, the only region of this phase diagram that has been realized experimentally in a photonic system is the low amplitude $W = +1$ region [3]. In this paper, we are concerned with whether we can realize a topological phase, residing in the strongly driven regime, for which the sign of the winding number is opposite to that of the weakly driven phase. When starting from the $W = +1$ regime and increasing the driving amplitude, the first two phases encountered are those in the $W = -2$ and $W = -1$ regions. In this paper, we will restrict our attention to the observation of the $W = -1$ phase and leave observation of higher winding number phases to future experiments. We comment that this $W = -1$ phase has been explored in cold atom experiments in the context of a dynamical phase transition following a quench between two Hamiltonians [28].

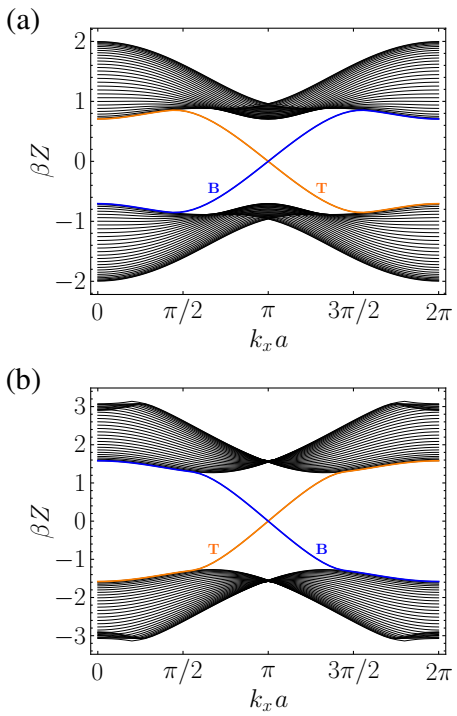

FIG. 3. Band structures for samples taken to be finite along the y-direction and periodic along the x-direction. The $W = +1$ phase is shown in (a) and the $W = -1$ phase in (b). These band structures are evaluated at the points in the phase diagram that correspond to the locations of the samples used in the experiment when operating at a wavelength of 1550 nm. Edge modes localized on the bottom (top) of the sample are labeled B (T) and are highlighted in blue (orange).

The $W = \pm 1$ phases that we observe here have a close relation to the two non-trivial phases of the Haldane model [24]. In particular, they persist at arbitrarily high frequencies where they can be understood by examining the inverse frequency expansion of the effective Floquet Hamiltonian [29], which reproduces the Hamiltonian of the Haldane model with an inversion symmetry breaking mass $M = 0$ and a time-reversal symmetry breaking parameter $\phi = \mathrm{sgn}(f)\pi/2$, with [20]

$$f(A) = \sum_{m\neq 0} \frac{J_m^2(A/\sqrt{3})\sin(2m\pi/3)}{m} \tag{3}$$

where $J_m(x)$ are the Bessel functions of the first kind. As a result, the winding number evaluates to either ± 1 and is selected by the sign of $f(A)$, which is in turn controlled by the amplitude of $\mathbf{A}(z)$.

To probe these two phases, we study the surface states associated with the bulk invariants [30]. Accordingly, a finite sample with counterclockwise waveguide chirality

taken from the $W = +1$ ($W = -1$) phase should possess a single counterclockwise (clockwise) edge mode traversing the gap centered on $\beta = 0$. Fig. 3 shows the tight binding band structures computed for each of the two phases using a strip geometry that is periodic in one direction and finite in the other. We see that in both cases the system is gapped with a single edge mode traversing the gap. The edge mode group velocity is reversed between the two cases, in agreement with the opposite sign of the associated bulk invariants.

To observe these edge modes experimentally, we fabricate two honeycomb lattices that each form a triangle with 17 waveguides on a side. Each side is terminated at a zig-zag edge. The structures are written in borosilicate glass with $n_0 = 1.473$ and $\delta n = 2.8 \times 10^{-3}$ using the femtosecond direct write technique [31]. We set the lattice constant to $a = 22\sqrt{3}\,\mu\text{m}$. The waveguides have diameters of 7.0 µm and 10.7 µm along the x and y directions and the sample length is 14 cm. The helix parameters for the two samples—which we will refer to as samples I and II—are respectively given by $(R_1, Z_1) = (20\,\mu\text{m}, 1.0\,\text{cm})$ and $(R_2, Z_2) = (106\,\mu\text{m}, 2.4\,\text{cm})$. In both samples, the helices are fabricated with counterclockwise helix chirality. For the purposes of comparing sample I with the sample in reference [3], please note that reference [3] uses clockwise helix chirality.

The locations of these samples on the phase diagram are wavelength dependent and are shown in Fig. 2 for wavelengths in the range 1480 nm to 1600 nm. Note that we have chosen the system parameters so that, at a wavelength of 1550 nm, the system is placed deep within the labeled topological phases such that, within fabrication tolerances, the system resides within the $W = \pm 1$ regions. We also note that while a system placed in the $W = -2$ phase would exhibit edge mode propagation similar to what we observe in our experiment for the $W = -1$ phase, the region of the $W = -2$ phase for which the group velocity is large enough to exhibit substantial propagation is narrow. Since our system has been placed significantly away from this region of parameter space, it is exceedingly unlikely that we have inadvertently accessed this region. In choosing the parameters for the large-radius sample, note that we have compensated for the additional loss that would be introduced upon increasing the helix radius by also increasing the period. As a result, the system lies well below the high-loss region, but as a by-product of attempting to satisfy the conflicting goals of moving to a new topological phase while minimizing losses, we have arrived in a counterintuitive regime where the diameter of a single helix is on the same scale as the size of the entire lattice.

To excite the edge modes, we shift the waveguides at the corners of the triangle so that their nearest neighbor spacing is a factor of 1.25 larger than the nearest neighbor spacing defining the lattice. In the weak coupling limit, these waveguides couple primarily to modes centered around $\beta = 0$ and hence excite the edge modes that cross the gap. We thus inject light at the corners, allow it to propagate through the structure, and then image it at the output facet using an InGaAs camera. The raw camera data is then converted to intensity data using a map obtained by calibrating against a tunable laser source of known intensity. The results are shown in Fig. 4, where we see a clear transition from counterclockwise to clockwise propagation.

While the propagation distance of the light is fixed for a given sample, we can effectively image the light at different stages of propagation by varying the group velocity of the edge mode. To accomplish this, we note that the tight-binding coupling constant is an increasing function of wavelength and, as a result, variation of the group velocity can be implemented via a wavelength sweep. Such a wavelength sweep simultaneously changes the coupling and shifts the system in the topological phase diagram along the paths shown in Fig. 2. In our experiment, we implement a sweep from 1480 nm to 1600 nm. Over this range, the system remains in the same topological phase while exhibiting an increased group velocity for larger wavelengths. As a result, the transverse distance traveled by the edge modes arriving at the output facet is observed to increase with wavelength (see Fig. 4 and Supplemental Material [32]).

DISCUSSION

We have considered a honeycomb array of helical waveguides operating in the paraxial limit and experimentally shown that we can access the strongly driven region of the Floquet topological phase diagram to observe a topological phase in which the winding number changes sign with respect to the weakly driven phase. We observed both the weakly and strongly driven phases by direct imaging of the associated chiral edge modes in a system with finite geometry. This observation demonstrates the accessibility of a large interval of the parameter space associated with the amplitude degree of freedom and shows the feasibility of future experimental realization of additional topological physics associated with a large drive amplitude, including higher winding number topological phases.

We also point out that, as the gauge field amplitude contains a wavelength dependence through the factor of k_0, the amplitude degree of freedom has the potential to enable wavelength sensitive selection of topological phases. Prior studies of such wavelength dependence have uncovered implications for three-dimensional systems, where features of the phase diagram for a two-dimensional system have been shown to underlie the emergence of Weyl points in an associated three-dimensional photonic band structure [23]. The accessibility of the strongly driven Floquet regime in photonics has the potential to enable explorations of a similar nature with potentially richer three-dimensional physics. The wavelength dependence of the gauge field amplitude could also serve as a basis for a robust topological wave-

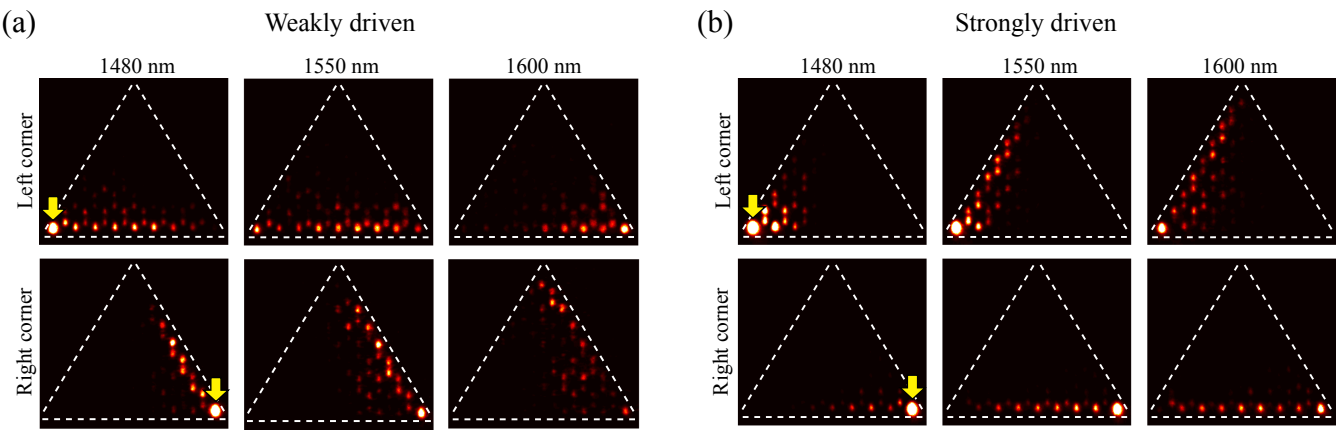

FIG. 4. Light arriving at the output facet after 14 cm of propagation. Panels (a) and (b) correspond, respectively, to samples that have been placed in the $W = +1$ (weakly driven, sample I) and $W = -1$ (strongly driven, sample II) regions of the phase diagram. Light is injected at the corner indicated by the arrow: the first (second) row corresponds to injection at the left (right) corner. Dashed white lines have been overlaid on the images to indicate the sample boundaries. By sweeping the wavelength, we effectively observe the light at different propagation distances along the sample (see text). A clear transition from counterclockwise to clockwise circulation is observed, consistent with the sign change of the bulk topological invariant.

length filter that utilizes the wavelength dependent chirality of the topological edge modes to direct light in a clockwise or counterclockwise fashion depending on its wavelength.

In moving into the strongly driven regime, one encounters the problem of bending losses that can be large enough to wash out the signatures of the topological physics. To overcome this difficulty, we effectively stretched the helices along the z-direction so as to lower the helix frequency while drastically increasing the helix radius in a way that simultaneously increases the waveguide curvature radius while keeping the system in the desired topological phase. This result goes beyond the photonic context discussed here in the sense that it may be applied to Floquet phases of two-dimensional solid-state materials (e.g., graphene). In particular, these ideas have direct application to the mitigation of heating and the engineering of topological phases in the intermediate and strongly driven regimes of Floquet systems.

ACKNOWLEDGMENTS

M.C.R. acknowledges the National Science Foundation under award number ECCS-1509546, the Charles E. Kaufman Foundation, a supporting organization of the Pittsburgh Foundation, and the Alfred P. Sloan Foundation under fellowship number FG-2016-6418. K.P.C. acknowledges the National Science Foundation under award numbers ECCS-1509199 and DMS-1620218.

[1] F. D. M. Haldane and S. Raghu, Phys Rev Lett **100**, 013904 (2008).
[2] Z. Wang, Y. Chong, J. D. Joannopoulos, and M. Soljacic, Nature **461**, 772 (2009).
[3] M. C. Rechtsman, J. M. Zeuner, Y. Plotnik, Y. Lumer, D. Podolsky, F. Dreisow, S. Nolte, M. Segev, and A. Szameit, Nature **496**, 196 (2013).
[4] M. Hafezi, S. Mittal, J. Fan, A. Migdall, and J. M. Taylor, Nat Photonics **7**, 1001 (2013).
[5] L. Lu, J. D. Joannopoulos, and M. Soljacic, Nat Photonics **8**, 821 (2014).
[6] X. Cheng, C. Jouvaud, X. Ni, S. H. Mousavi, A. Z. Genack, and A. B. Khanikaev, Nat Mater **15**, 542 (2016).
[7] G. Jotzu, M. Messer, R. Desbuquois, M. Lebrat, T. Uehlinger, D. Greif, and T. Esslinger, Nature **515**, 237 (2014).
[8] M. Aidelsburger, M. Lohse, C. Schweizer, M. Atala, J. T. Barreiro, S. Nascimbene, N. R. Cooper, I. Bloch, and N. Goldman, Nat Phys **11**, 162 (2015).
[9] N. Goldman, J. C. Budich, and P. Zoller, Nat Phys **12**, 639 (2016).
[10] E. Prodan and C. Prodan, Phys Rev Lett **103**, 248101 (2009).
[11] L. Zhang, J. Ren, J.-S. Wang, and B. Li, Phys Rev Lett **105**, 225901 (2010).
[12] C. L. Kane and T. C. Lubensky, Nat Phys **10**, 39 (2014).
[13] L. M. Nash, D. Kleckner, A. Read, V. Vitelli, A. M. Turner, and W. T. M. Irvine, Proc Natl Acad Sci **112**, 14495 (2015).
[14] S. D. Huber, Nat Phys **12**, 621 (2016).
[15] A. Szameit and S. Nolte, Journal of Physics B: Atomic, Molecular and Optical Physics **43**, 163001 (2010).
[16] T. Oka and H. Aoki, Phys Rev B **79**, 081406 (2009).
[17] T. Kitagawa, E. Berg, M. Rudner, and E. Demler, Phys

Rev B **82**, 235114 (2010).
[18] N. H. Lindner, G. Refael, and V. Galitski, Nat Phys **7**, 490 (2011).
[19] Z. Gu, H. A. Fertig, D. P. Arovas, and A. Auerbach, Phys Rev Lett **107**, 216601 (2011).
[20] T. Mikami, S. Kitamura, K. Yasuda, N. Tsuji, T. Oka, and H. Aoki, Phys Rev B **93**, 144307 (2016).
[21] M. S. Rudner, N. H. Lindner, E. Berg, and M. Levin, Phys Rev X **3**, 031005 (2013).
[22] D. Leykam, M. C. Rechtsman, and Y. D. Chong, Phys Rev Lett **117**, 013902 (2016).
[23] J. Noh, S. Huang, D. Leykam, Y. D. Chong, K. P. Chen, and M. C. Rechtsman, Nat Phys **13**, 611 (2017).
[24] F. D. M. Haldane, Phys Rev Lett **61**, 2015 (1988).
[25] C.-Z. Chang, J. Zhang, X. Feng, J. Shen, Z. Zhang, M. Guo, K. Li, Y. Ou, P. Wei, L.-L. Wang, Z.-Q. Ji, Y. Feng, S. Ji, X. Chen, J. Jia, X. Dai, Z. Fang, S.-C. Zhang, K. He, Y. Wang, L. Lu, X.-C. Ma, and Q.-K. Xue, Science **340**, 167 (2013).
[26] T. Fukui, Y. Hatsugai, and H. Suzuki, Journal of the Physical Society of Japan **74**, 1674 (2005).
[27] D. Marcuse, J Opt Soc Am **66**, 216 (1976).
[28] N. Fläschner, D. Vogel, M. Tarnowski, B. S. Rem, D.-S. Lühmann, M. Heyl, J. C. Budich, L. Mathey, K. Sengstock, and C. Weitenberg, Nat Phys (2017).
[29] M. Bukov, L. D'Alessio, and A. Polkovnikov, Adv Phys **64**, 139 (2015).
[30] M. Z. Hasan and C. L. Kane, Rev Mod Phys **82**, 3045 (2010).
[31] K. M. Davis, K. Miura, N. Sugimoto, and K. Hirao, Opt Lett **21**, 1729 (1996).
[32] See Supplemental Material at URL for animations showing the full wavelength sweep.